Fluid inerter for optimal vibration control of floating offshore wind turbine towers

Downloaded from: https://research.chalmers.se, 2026-10-12 16:15 UTC

Citation for the original published paper (version of record):
Sarkar, S., Fitzgerald, B. (2022). Fluid inerter for optimal vibration control of floating offshore wind turbine towers. Engineering Structures, 266. http://dx.doi.org/10.1016/j.engstruct.2022.114558

N.B. When citing this work, cite the original published paper.

research.chalmers.se offers the possibility of retrieving research publications produced at Chalmers University of Technology. It covers all kind of research output: articles, dissertations, conference papers, reports etc. since 2004. research.chalmers.se is administrated and maintained by Chalmers Library

(article starts on next page)

Engineering Structures 266 (2022) 114558

Contents lists available at ScienceDirect

Engineering Structures

journal homepage: www.elsevier.com/locate/engstruct

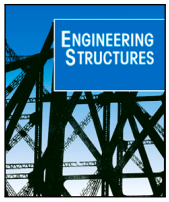

Fluid inerter for optimal vibration control of floating offshore wind turbine towers

Saptarshi Sarkar [a], Breiffni Fitzgerald [b,*]

[a] Department of Mechanics and Maritime Sciences, Chalmers University of Technology, Gothenburg, Sweden
[b] School of Engineering, Trinity College Dublin, Ireland

ARTICLE INFO

Keywords:
Inerter
Tuned mass damper
Tuned mass damper fluid inerter (TMDFI)
Vibration control
Non-linear optimization
Stochastic wind-wave loads
Spar-type floating offshore wind turbine

ABSTRACT

This paper proposes the use of a tuned mass damper fluid-inerter (TMDFI) for vibration control of spar-type floating offshore wind turbine towers. The use of an inerter in parallel with the spring and damper of a tuned mass damper (TMD) is a relatively new concept. The ideal inerter has a mass amplification effect on the classical TMD leading to greater vibration control capabilities. Previous work by the authors has shown that inerter based TMDs have great potential in vibration control of floating offshore wind turbines where enhanced vibration mitigation can be achieved using a relatively lighter device than classical TMDs. However, this previous work was based on the assumption of an ideal inerter that assumes the use of a mechanical flywheel type inerter. Mechanical inerters have some inherent disadvantages due to their complexity in design and high cost of maintenance. The use of a fluid inerter can alleviate these disadvantages as its design is rather simple and it comes with very low maintenance. Such devices have been proposed and investigated in the literature, however, their applicability in vibration control of floating wind turbines has not been investigated by researchers. The optimal design of a TMDFI is presented in this paper. It has been shown that optimization of a TMDFI is a six-dimensional non-linear optimization problem whose solution hyperplane contains multiple local minima. A systematic way has been developed in this paper, avoiding the use of metaheuristic search techniques, to optimize the damper while providing greater insight into the damper properties that offers a set of guidance to the designer. Numerical results demonstrate impressive vibration control capabilities of this new device under various stochastic wind-wave loads. It has been shown that the fluid-inerter performs as well as the ideal mechanical inerter. The considerable advantages of a TMDFI over the classical TMD demonstrated in this paper makes it an exciting candidate for vibration control.

1. Introduction

The progress of the wind energy industry in the past decade has been remarkable. The total global installed wind energy capacity now stands at over 743 gigawatts (GW) in 2021 compared to 197 GW in 2010 [1]. The large increases in capacity have been brought about by developments in wind turbine technology and the associated reduction in the cost of wind energy. Wind turbine research and development has progressed the state-of-the-art from a 10 m diameter, 10 kW turbine in the 1980s to machines which are now the largest rotating structures on Earth with diameters approaching 200 m diameter and capacities of 15 MW. Global wind energy penetration is currently estimated at 5% and recent research by the International Renewable Energy Agency (IRENA) projects that by 2050 wind energy could provide 35% of the world's installed electricity, becoming the planet's largest energy source and the backbone of power systems [2]. However, there remain technical challenges to be overcome in order to realize these projections.

The future of wind energy lies offshore. The cost of offshore wind turbine foundations is about 45% of the wind turbine cost in shallow water depths [3]. Since the wind resource improves with distance offshore, it is desirable for installations to be sited far offshore in deep waters. However, the cost for foundations at the water depths of 40–50 m is 1.9 times higher than the cost for the water depth of 10–20 m. In order to reduce the cost of offshore wind energy the concept of floating offshore wind turbines (FOWTs) has been investigated by researchers in recent years. FOWTs are proposed for deep offshore installations and have been realized in recent years in offshore wind farms in Scotland (Hywind) and Portugal (Windfloat). FOWTs present additional challenges to traditional onshore or fixed base offshore turbines. FOWTs are very large flexible structures installed in very harsh environments. These structures are subjected to turbulent aerodynamic and hydrodynamic loads. The stability of the FOWT (pitching

* Corresponding author.
E-mail addresses: ssarkar@chalmers.se (S. Sarkar), breiffni.fitzgerald@tcd.ie (B. Fitzgerald).

https://doi.org/10.1016/j.engstruct.2022.114558
Received 23 November 2020; Received in revised form 31 January 2022; Accepted 13 June 2022
Available online 27 June 2022
0141-0296/© 2022 The Author(s). Published by Elsevier Ltd. This is an open access article under the CC BY license (http://creativecommons.org/licenses/by/4.0/).

and rolling of the platform) is an important aspect that must also be considered. Mitigating the structural vibrations of FOWTs is now a very active area of research since vibrations of the blades and towers of FOWTs will affect the power production [4] and will also affect the reliability of the structures [5]. There have been many different vibration control schemes proposed to reduce vibrations in offshore wind turbines. Passive control via tuned mass dampers [6–9], tuned liquid column dampers [10] and pendulum dampers [11,12] has been proposed. Semi-active [13–16] and active [17–21] control has also been investigated by researchers. The possibility of using already installed pitch controllers [22–24] and generator torque controllers [25] to control vibrations in FOWTs has also been considered in recent studies.

Some wind turbine vibration control studies have made use of recent developments in damper design due to the emergence of the so-called 'inerter'. The inerter was originally proposed by Smith [26] as a two-terminal mechanical device analogous to the capacitor in electrical systems. The inerter has the property that the equal and opposite force applied at the nodes is proportional to the relative acceleration between the nodes. The inerter has been applied in recent vibration control studies and it is often used in novel TMD configurations [27–30]. Inerter based dampers can provide a mass amplification effect which increases the effective mass of the device, thus improving its vibration control performance. Recently there have been studies done on the use of inerter-based dampers for vibration control of offshore wind turbines. All of these studies involved variations of different inerter-based TMD devices. Onshore [31,32], offshore [33] and floating offshore [34–36] wind turbines have been considered.

All of the inerter-based dampers investigated to date in the wind turbine literature have made use of mechanical inerters, realized via gearing systems, rack and pinion assemblies, or other mechanical components. However, it is possible to realize the inertance without a mechanical inerter. Fluid based inerters were first proposed by Swift et al. [37] and in recent studies, these devices have been proposed for vibration control of large structures [38,39]. Fluid inerters have obvious advantages over mechanical devices. They are simple in design and can be readily adapted to implement different damper designs/layouts. Fluid inerters are also comparable in size to their mechanical counterparts. There are many parasitic effects that are typically neglected in mechanical inerter modelling/design such as ratcheting, backlash and friction phenomena [40]. These parasitic effects can be largely mitigated by using a fluid inerter. The fluid inerter can reduce the parasitic effects that are more pronounced in mechanical devices and also has greater inherent damping due to the fluid viscosity and density [38]. The fluid inerter can be modelled as an ideal inerter in parallel with a nonlinear parasitic damping component, this damping can be calculated from the damper geometry and fluid properties [37,41]. No study to date has investigated the use of a fluid inerter for a wind turbine application.

In this paper, we propose the use of a tuned mass damper fluid-inerter (TMDFI) for vibration control of a spar-type floating offshore wind turbine tower. Previous work by the authors has shown that inerter based tuned mass dampers have great potential in vibration control of floating offshore wind turbines where enhanced vibration mitigation can be achieved using a relatively lighter device [36]. However, this previous work was based on the assumption of an "ideal" inerter that assumes the use of a mechanical flywheel type inerter. Rotating mechanical systems, such as inerters, have some inherent disadvantages due to their complexity in design and the high cost of maintenance. The use of a fluid inerter can alleviate these disadvantages as its design is rather simple and it comes with very low maintenance. In this paper, the controller (TMDFI) is first designed systematically using a reduced degree of freedom tower-TMDFI coupled system in Section 3 highlighting the properties of the fluid-inerter. Then, the performance of the damper is evaluated by coupling it to a full-scale 5MW floating offshore wind turbine and the results are presented in Section 4. The spar-type floating offshore wind turbine model is briefly described next.

2. Offshore wind turbine coupled with TMDFI

A high-fidelity multi-body dynamic model of the floating offshore wind turbine (FOWT) coupled with a TMDFI is developed using Kane's method [42] for numerical investigation in the paper. State of the art wind turbine simulation tools like FAST [43] also employs Kane's method to model offshore wind turbines. This method presents a powerful vector approach that offers considerable advantages over the traditional Euler–Lagrangian formulation as the equations of motion are obtained directly from the kinematic description of a system. This is particularly advantageous for complicated systems like the (FOWT). Therefore, a description of the kinematics of the system instead of the total energy is enough to be able to derive the governing equations of motion.

For proper modelling of a multi-body system like an offshore wind turbine, it is necessary that every component is defined in its local coordinate system and then referred back to the global, in this case, inertial reference frame. Hence, local coordinate systems are assigned to the platform, tower nodes, tower-top, nacelle, low-speed shaft and the blades. The blades have more than one coordinate system assigned to them. For detailed modelling of the blades, they are projected to their coned coordinate system followed by the pitched coordinate system. Aerodynamic loads are applied on the blade nodes that are not only coned and pitched but also rotated due to elastic deformation of the blades in out-of-plane and in-plane directions. The coordinate systems used (except the tower and blade element fixed coordinate systems) are shown in Fig. 1. The platform rotation and rotation of the elastic members (tower and blades) occurs simultaneously about more than one axis. This restricts the use of a simple Euler rotation matrix to establish transformation relations between two coordinate systems. Although advanced methods can be used to derive these transformation relations, the small magnitude of these angles allows the use of small-angle approximation that makes an Euler 1-2-3 rotation matrix independent of the sequence of rotation. The resulting transformation matrix is not orthogonal, hence, singular value decomposition (SVD) is used to obtain the nearest orthogonal transformation. For details on the coordinate systems and kinematics of the FOWT please refer [44,45]

By a direct result of Newton's law of motion, Kane's equations of motion for a simple holonomic multi-body system can be stated as [42]

$$F_k + F_k^* = 0 \qquad \text{for } k = 1, 2, \dots N \tag{1}$$

where, N is the total number of degrees of freedom required to describe the complete kinematics of the wind turbine system. With a set of M rigid bodies characterized by reference frame N_i and centre of mass point X_i, the *generalized active force* associated with the kth degree of freedom is given as [42]

$$F_k = \sum_{i=1}^{M} \left[{}^E\mathbf{v}_k^{X_i} \cdot \mathbf{F}^{X_i} + {}^E\boldsymbol{\omega}_k^{N_i} \cdot \mathbf{M}^{N_i} \right] \tag{2}$$

where $\mathbf{F}^{X_i}$ is force vector acting on the centre of mass of point X_i and $\mathbf{M}^{N_i}$ is the moment vector acting on the N_i rigid body. ${}^E\mathbf{v}_k^{X_i}$ and ${}^E\boldsymbol{\omega}_k^{N_i}$ are the partial linear and partial angular velocity of the point X_i and rigid body N_i respectively associated with the kth degree of freedom in the inertial (E) reference frame. The *generalized inertia force* for kth degree of freedom is given as

$$F_k^* = -\sum_{i=1}^{M} \left[{}^E\mathbf{v}_k^{X_i} \cdot \left(m^{N_i} {}^E\mathbf{a}^{X_i} \right) + {}^E\boldsymbol{\omega}_k^{N_i} \cdot {}^E\dot{\mathbf{H}}^{N_i} \right] \tag{3}$$

where it is assumed that for each rigid body N_i, the inertia forces are applied at the centre of the mass point X_i. ${}^E\dot{\mathbf{H}}^{N_i}$ is the time derivative of the angular momentum of rigid body N_i about its centre of mass X_i in the inertial frame [42]. For the wind turbine model, the mass of the platform, tower, yaw bearing, nacelle, hub, blades, generator contributes to the total generalized inertia forces. Generalized active

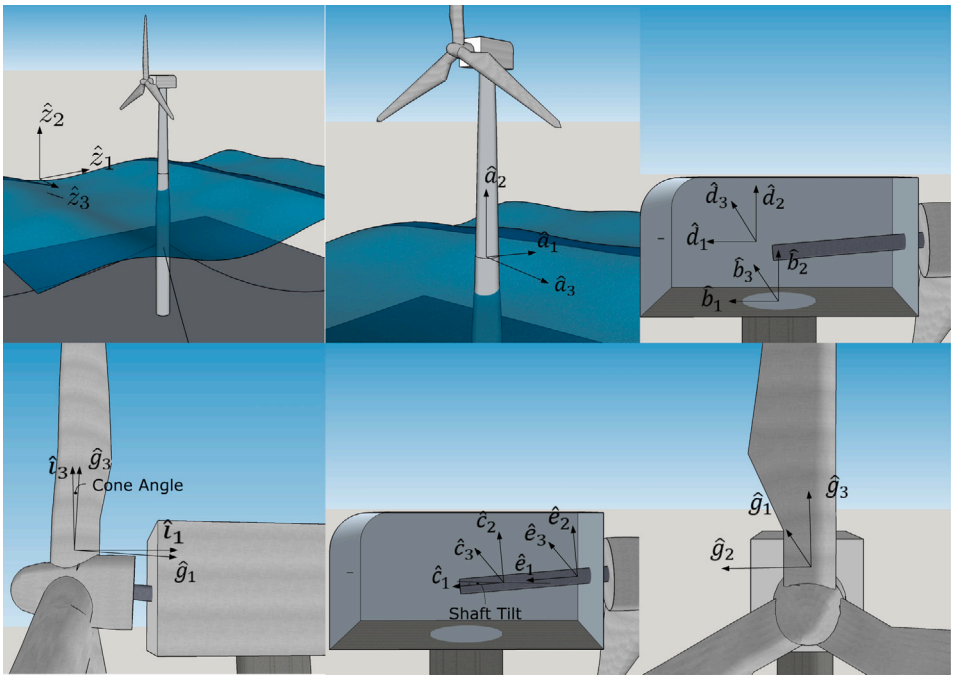

Fig. 1. Coordinate systems for FOWT.

forces are the forces applied directly to the wind turbine system, forces that ensure constraint relationships between the various rigid bodies and internal forces within flexible members. Forces applied directly on the offshore wind turbine system include aerodynamic forces on the blades and the tower, hydrodynamic forces on the platform, mooring forces on the platform, gravitational forces, generator torque, high-speed shaft brake. Here it must be noted that gearbox friction forces are neglected. Yaw springs and damper contribute to forces that enforce constraint relationship between rigid bodies. Internal forces within flexible members include elasticity and damping in the tower, blades and drivetrain.

As can be observed from the above equations, the kinematic description, i.e., the position, velocity and acceleration vectors of all important points on the offshore wind turbine system is the key requirement. As shown in Fig. 2, the TMDFI is placed at the tower-top denoted by the point O, and hence the position vector of the damper from the tower-top can be given as

$$r^{OD} = \begin{cases} q_D \hat{\mathbf{b}}_3 & \text{coupled to side-to-side direction} \\ q_D \hat{\mathbf{b}}_1 & \text{coupled to fore–aft direction} \end{cases} \tag{4}$$

where D denotes the centre of mass of the damper and q_D is the displacement of the damper from its neutral position. The kinematics of the coupled system is derived which, although straightforward, can be extensive due to the complexity of the overall system. The mass of the damper contributes to the generalized inertia forces and the spring, damper and inerter contribute to the generalized active forces of the entire system. To describe the complete motion of the coupled offshore wind turbine TMDFI system the degrees of freedom/generalized coordinates used are given in Eq. (5).

$$\mathbf{q} = \{q_{Sg}\ \ q_{Sw}\ \ q_{Hv}\ \ q_R\ \ q_P\ \ q_Y\ \ q_{TFA1}\ \ q_{TSS1}\ \ q_{TFA2}\ \ q_{TSS2}\ \ q_{yaw}\ \ q_{GeAz}\ \ q_{DrTr}\ \ q_{B1F1}\ \ q_{B1E1}\ \ q_{B1F2}\ \ q_{B2F1}\ \ q_{B2E1}\ \ q_{B2F2}\ \ q_{B3F1}\ \ q_{B3E1}\ \ q_{B3F2}\ \ q_D\} \tag{5}$$

The subscripts define the degrees of freedom under consideration and are described in Appendix. Once the linear and angular velocity vectors for every important point and rigid body in the system are defined, the partial linear and angular velocities are obtained as per [42] using the time derivatives of the generalized coordinates as the generalized speed (i.e., $u_k = \dot{q}_k$). The complete non-linear time-domain equations of motion for the offshore wind turbine system in its general form can be written as

$$\mathbf{M}(\mathbf{q}, \mathbf{u}, t)\dot{\mathbf{q}} = -\mathbf{f}(\dot{\mathbf{q}}, \mathbf{q}, \mathbf{u}, t) \tag{6}$$

where, $\mathbf{M}$ is the inertial mass matrix that is a non-linear function of the set of degrees of freedom $\mathbf{q}$, control input $\mathbf{u}$, and time t. The force vector $\mathbf{f}$ depends non-linearly on the degrees of freedom, the time derivative of the degrees of freedom, control input and time. For details on the derivation of the equations of motion please refer [44,45]. The FOWT model without the coupled damper has been benchmarked and verified against the National Renewable Energy Laboratory's (NREL) fully coupled nonlinear simulation code, FAST [43] in [23,36].

Table 1
TMDFI parameters.

Parameter	Description	Selected values
D_c	Cylinder diameter	1.75 m
D_h	Helix diameter	0.20 m
R	Bent radius of helix	1.0 m
ω_r	Tuning ratio	9.58
ζ_d	Damping ratio	0.00
l	Length of the cylinder	1.50 m
β	Inerter ratio	0.715
ρ	Fluid density	997 kg/m^3
μ_f	Fluid dynamic viscosity	0.0009 Pa s

3. Controller design based on a reduced 2-DOF system

The coupled offshore wind turbine TMDFI system described above is a 23-DOF non-linear system. While it is possible to optimize the 23-DOF non-linear system using meta-heuristic search techniques, these methods are highly computationally inefficient and especially disadvantageous during the conceptual development phase of a device. This issue is alleviated using a lower degree of freedom (DOF) system to identify the dominant mode of a structure, i.e., the natural frequency of the tower in this case, and to subsequently design a damper to suppress this using the lower DOF system. The primary reason for using

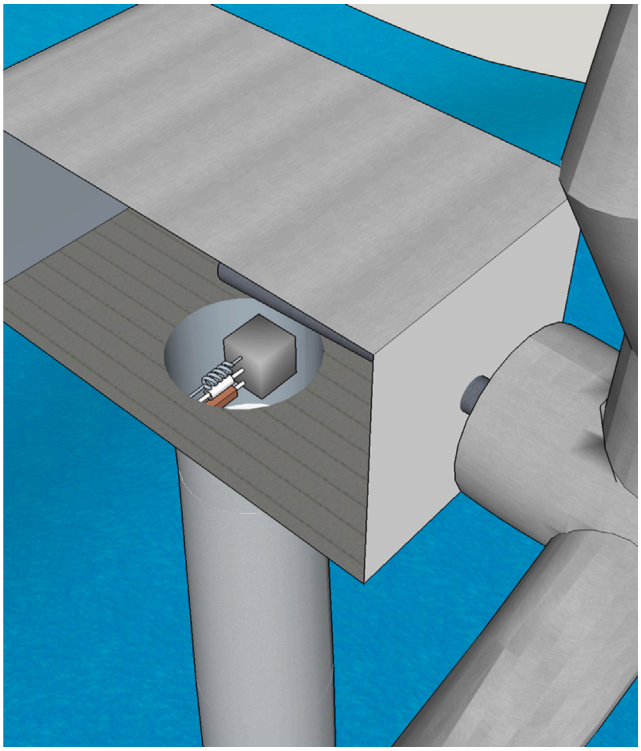

Fig. 2. Floating offshore wind turbine with TMDFI.

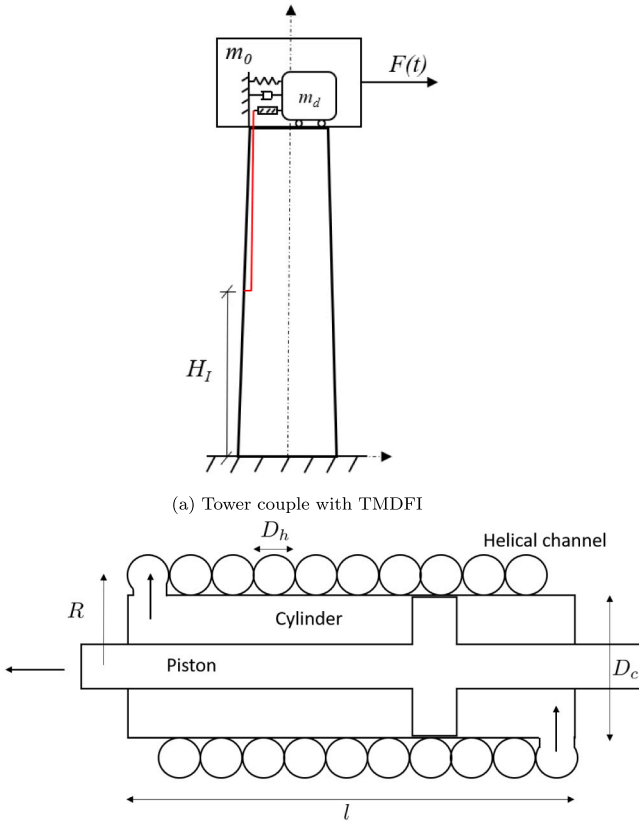

(a) Tower couple with TMDFI

(b) Fluid inerter

Fig. 3. Schematic diagram of the tower and fluid inerter.

this method is — the environmental loading is broad banded/coloured and highly intermittent in nature, therefore the tower vibrations are dominated its natural frequency over its design life. The method is standard structural control and has been used time and again by researchers [14,36,46–50]. Using a similar approach, the optimal properties of the TMDFI are derived using a reduced degree of freedom model. However, it must be noted that the parasitic damping offered by the fluid inerter [37] is non-linear in nature and is a function of the relative velocity of the damper mass and the point of connection on the tower. This renders the reduced 2-DOF model non-linear and makes the use of linear dynamics or other linearization approaches infeasible. Therefore, the problem at hand is a 2-DOF non-linear system, for which the optimal damper parameters need to be identified. The primary aim of the design procedure is to develop a computationally efficient way of designing the damper and to provide insight into the damper's behaviour. With this in mind, first, the equations of motion of the reduced 2-DOF system are presented followed by optimization of the damper in the subsequent subsections.

3.1. Equations of motion of the 2-DOF system

The simplified model of a tower with a TMDFI placed on its top is shown in Fig. 3(a) and a schematic diagram of the fluid inerter is presented in Fig. 3(b). It is assumed that the mass of the blades, hub and nacelle are lumped on the top of the tower and the base of the tower is fixed. The inerter is hooked between the mass of the damper and the tower at an arbitrary height H_I from the base of the tower. For such a system, the governing equations of motion, normalized by the mass of the primary structure m_0, is given as

$$\begin{bmatrix} 1+\mu+\beta(1-\phi)^2 & \mu+\beta(1-\phi) \\ \mu+\beta(1-\phi) & \mu+\beta \end{bmatrix} \begin{pmatrix} \ddot{q}_t \\ \ddot{q}_d \end{pmatrix} + \begin{bmatrix} 2\omega_t\zeta_t & 0 \\ 0 & 2\mu\omega_t\zeta_d\omega_r \end{bmatrix} \begin{pmatrix} \dot{q}_t \\ \dot{q}_d \end{pmatrix} + \begin{bmatrix} \omega_t^2 & 0 \\ 0 & \mu\omega_t^2\omega_r^2 \end{bmatrix} \begin{pmatrix} q_t \\ q_d \end{pmatrix} + \begin{pmatrix} (1-\phi)F_d(v) \\ F_d(v) \end{pmatrix} = \frac{1}{m_0} \begin{pmatrix} F_w \\ 0 \end{pmatrix} \tag{7}$$

The tower and damper degrees of freedom are denoted by q_t and q_d respectively. The mass ratio of μ and inerter ratio β are defined as

$$\mu = \frac{m_d}{m_0} \qquad \beta = \frac{b}{m_0} \tag{8}$$

where m_d is the mass of the damper and b is the constant of proportionality of the force generated by the inerter. It has the units of mass and details on this parameter can be found in [51,52]. The natural frequency of the tower and damper is denoted by ω_t and ω_d respectively. The tuning ratio and damping ratio of the damper are defined as

$$\omega_r = \frac{\omega_d}{\omega_t} \qquad \zeta_d = \frac{c_d}{2m_d\omega_d} \tag{9}$$

where c_d is the damping coefficient of the TMDFI. ϕ is the normalized displacement ratio between tower top displacement and the displacement at a height H_I from the base. It can be obtained directly from the normalized primary mode shape as

$$\phi = \phi_t(H_I) \qquad \text{where } 0 \le \phi \le 1 \tag{10}$$

where, ϕ_t is the normalized primary mode shape of the tower. F_w is the wind excitation force. F_d is the nonlinear parasitic damping of the fluid inerter given as [37]

$$F_d(v) = 0.03426\frac{2\rho l A_c}{\sqrt{D_h R}}\left(\frac{A_c}{A_h}\right)^2 v|v| + 17.54\frac{2\mu_f l A_c}{D_h^2}\left(\frac{A_c}{A_h}\right)v \tag{11}$$

The description of the different parameters in the above equation are given in Table 1. The relative velocity v is given as

$$v = \dot{q}_d - \phi\dot{q}_t \tag{12}$$

The fluid inerter's inertance is given as [37]

$$b = \rho l \frac{A_c^2}{A_h} \tag{13}$$

Normalized parasitic damping of the fluid inerter can be obtained as

$$\bar{F}_d = 0.06852 \frac{D_c^2 \beta}{D_h^{5/2}\sqrt{R}} v|v| + 35.08 \frac{\mu_f \beta}{D_h^2 \rho} v \tag{14}$$

3.2. A discussion on the solution approach

The design of the damper presented above requires optimization of six parameters (D_c, D_h, R, l, ω_r and ζ_d), and therefore presents an six-dimensional optimization problem. A common method to solve the optimization problem is to first define a cost function as the root mean square (RMS) value of the tower response (typically the displacement) obtained from time history predictions (typically 10 min long). This cost function is then optimized using non-linear optimization tools to find the global minimum. However, there are two potential issues with this approach, identified as

1. Using time-domain simulations to evaluate the cost function in the non-linear optimization algorithm is computationally expensive.
2. Authors in [46,53,54] have reported that gradient-based non-linear optimization tools such as Sequential Quadratic Programming (SQP) perform poorly in solving the constrained optimization problem of identifying the optimal damper parameters due to the presence of multiple local minima of the solution hyperplane. This observation was also confirmed in this paper. SQP failed to find the global minima of the six-dimensional optimization problem due to the presence of multiple local minima.

Hence, to solve the optimization problem global search tools are required and the use of Genetic Algorithms (GA) has seen rapid growth in the wind energy industry. For example, GA has been used by Stewart and Lackner [46] to optimize the TMD parameters when the stroke of the TMD was constrained by the available space on the turbine. The authors showed that SQP failed to find the global minimum and global optimization tools like GA are needed. In [53,54], the authors also used GA to find the optimal parameters of a constrained TMD and reported that GA performs better than other methods such as the exhaustive search method. However, the motivation to not use GA or the likes in this paper is two fold:

1. GA suffers from being extremely computation expensive for an offshore wind turbine system. In the time domain, every realization of the time histories is generated using a unique random seed. Therefore, a time-domain optimized result, in theory, should be the average of a sufficiently large number of random seeds. Even though the computation time is not the limiting factor for a damper that is optimized offline, it does present a limitation during the conceptual development phase of the device if every instance of parameter change requires hours of computation time.
2. All insight into the optimization problem (damper behaviour in this case) is lost. This is particularly disadvantageous because the use of a fluid-inerter for vibration control of floating offshore wind turbine towers is the first of its kind. Therefore, the impact of every parameter must be properly understood.

Therefore, to reduce simulation time, the response of the system was examined in the frequency domain using an extended harmonic balance method (EHBM). The frequency response of the 2-DOF system obtained from EHBM is used to optimize the TMDFI. And, to investigate the impact of each parameter a structured sensitivity analysis used leading to the optimal design of the damper. The extended harmonic balance method is briefly summarized next.

3.3. Frequency response analysis using extended harmonic balance method

This section provides a brief description of the harmonic balance method used in this paper for frequency response analysis of the 2-DOF system. The reader should refer to a specialized text such as [55] for details on the harmonic balance method. The section concludes by defining a cost function that quantifies the performance of the fluid inerter for a given set of parameters.

The mechanical system in Eq. (7) can be written in the form

$$\mathbf{M}\ddot{\mathbf{q}} + \mathbf{D}\dot{\mathbf{q}} + \mathbf{K}\mathbf{q} + \mathbf{f}_{nl}(\dot{\mathbf{q}}, \mathbf{q}) = \mathbf{f}_{ex}(t) \tag{15}$$

where, $\mathbf{q}$, $\mathbf{f}_{nl}$, $\mathbf{f}_{ex} \in \mathfrak{R}^{n\times 1}$ are vectors of generalized coordinates, nonlinear forces and external forces; and n is the number of degrees of freedom. Assuming that the external force is periodic in nature $\mathbf{f}_{ex}(t) = \mathbf{f}_{ex}(t+T)$, the assumed periodic solution (ansatz) is written in the form of a Fourier series

$$\begin{aligned}\mathbf{q}_h(t) &= \mathbf{Q}_0 + \sum_{k=1}^{\infty}\left[\mathbf{Q}_{c,k}\cos(k\omega t) + \mathbf{Q}_{s,k}\sin(k\omega t)\right] \\ &= \mathfrak{R}\left\{\sum_{k=0}^{\infty}\mathbf{Q}_k e^{ik\omega t}\right\}\end{aligned} \tag{16}$$

The coefficients $\mathbf{Q}_{c,k}$ and $\mathbf{Q}_{s,k}$ are real valued, whereas, the coefficients $\mathbf{Q}_k$ are complex valued. Substituting, Eq. (16) and its first and second order time derivative in Eq. (15) a residue can be quantified as

$$\mathbf{R} = \mathfrak{R}\left\{\sum_{k=0}^{\infty}\left(\left[-(k\omega)^2\mathbf{M} + ik\omega\mathbf{D} + \mathbf{K}\right]\mathbf{Q}_k + \mathbf{F}_{nl,k} - \mathbf{F}_{ex,k}\right)e^{ik\omega t}\right\} \tag{17}$$

Here, it is assumed that a Fourier expression for a excitation force is available in the form

$$\mathbf{f}_{ex} = \mathfrak{R}\left\{\sum_{k=0}^{\infty}\mathbf{F}_{ex,k}e^{ik\omega t}\right\} \tag{18}$$

and the nonlinear forces are sufficiently smooth in $\mathbf{q}_h$ and $\dot{\mathbf{q}}_h$ and can also be approximated by a Fourier series. The residue for the k^{th} harmonic is given as

$$\mathbf{R}_k = \left[-(k\omega)^2\mathbf{M} + ik\omega\mathbf{D} + \mathbf{K}\right]\mathbf{Q}_k + \mathbf{F}_{nl,k} - \mathbf{F}_{ex,k} \tag{19}$$

The Fourier coefficient is usually truncated to an order H to arrive at H number of equations with H unknowns where, $\mathbf{R}_0$, $\mathbf{Q}_0 \in \mathfrak{R}^{n\times 1}$ and $\mathbf{R}_k$, $\mathbf{Q}_k \in \mathbb{C}^{n\times 1}$ for $k = 1$ to H. Eq. (19) is a set of nonlinearly coupled algebraic equations and the governing equation of the harmonic balance method. Generally, increasing the harmonic order H increases the solution accuracy at a cost of increased computational effort. Therefore, the truncation order must be chosen in such a way that it offers sufficient accuracy without incurring inordinate computational effort.

Another important aspect of the harmonic balance method is the resolution of the nonlinear forces. The most popular method used to resolve the nonlinear forces is the Alternating-Frequency-Time (AFT) method. In this method, the Fourier transformation of the nonlinear forces is replaced by discrete Fourier transform. The procedure can be summarized mathematically as

$$\mathbf{F}_{nl,k} = \text{FFT}\left[\mathbf{f}_{nl}\left(\text{iFFT}\left\{\mathbf{Q}_k\right\},\ \text{iFFT}\left\{ik\omega\mathbf{Q}_k\right\}\right)\right] \tag{20}$$

In Eq. (20) the displacements and velocities are sampled at equal distances within one time period using the discrete inverse Fourier transform. Then the nonlinear force is sampled at the same time points and finally, the Fourier coefficients of the nonlinear forces are obtained using a discrete Fourier transform. The number of samples per period must be sufficiently large to resolve the highest harmonic in accordance with the Nyquist-Shannon theorem. In this paper, a sufficiently large number of samples is used to ensure all relevant harmonics are captured.

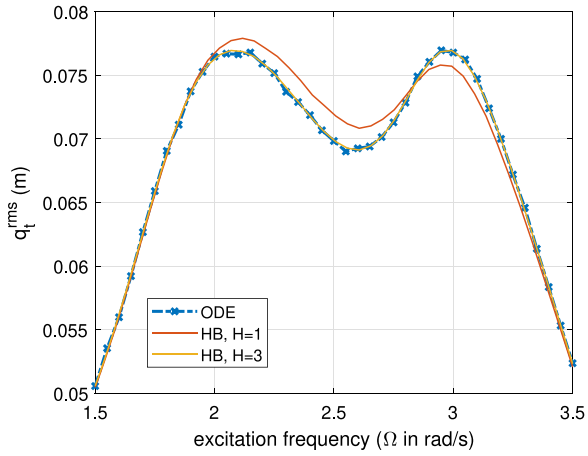

Fig. 4. Convergence of harmonic balance solution to time domain solution.

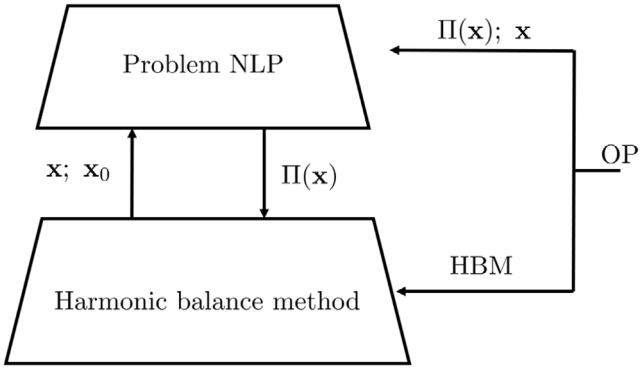

Fig. 5. Computation hierarchy and communication of data between two sub-problems

The most common methods used to minimize the residue (error) in Eq. (19) belong to the family of Newton-like methods. In this paper, the MATLAB function `fsolve` is used for this purpose. The Newton method is a gradient-based method that required an estimation of the Jacobian $\partial R/\partial x$. The Jacobian is approximated using a finite difference scheme here.

To find the solution of the harmonic balance method, a numerical path continuation method is used. A numerical path continuation method increases the robustness and efficiency of the numerical solution, especially in ranges with strong gradients (e.g., near resonances). The predictor–corrector continuation method is used here with arclength parametrization. In the predictor step, a step is taken along the tangent of the solution branch. The arclength parametrization enforces the solution point to be on the surface of a hypersphere with radius Δs through the previous solution point. The predicted step is generally not the solution point. Then, in the corrector step, `fsolve` is used to iteratively move towards the solution point. It is worth mentioning here that numerical path continuation techniques are a vast subject by itself and the interested reader may refer to a specialized text like [56] for details.

The last important aspect for consideration is the step length control. The step length is controlled in such a way that ensures fast convergences without overlooking important characteristics of the solution. When the solution curve is rather flat the step length increases and when the solution is near turning points the step length is reduced appropriately.

The convergence of the harmonic balance solution to the time domain ODE solution is shown in Fig. 4. It can be observed that convergence is achieved at $H = 3$ and hence a harmonic order of 3 has been used in this paper. The root-mean-square (RMS) displacement of the system is obtained from the harmonic coefficients on the solution branch as

$$\mathbf{a}_{rms} = \sqrt{\mathbf{R}_0^2 + \frac{\sum_{k=1}^{H} |\mathbf{R}_k|^2}{2}} \tag{21}$$

A cost function is defined as the infinity norm of the tower frequency response curve, which in other words is the peak of the frequency response curve. The cost function is given as

$$\Pi(\mathbf{x}) = \|q_t^{rms}\|_\infty \qquad q_t^{rms} = \mathbf{a}_{rms}^{(1)} \tag{22}$$

The cost function is a function of the tuning ratio and the damping ratio ($\mathbf{x} = [\omega_r\ \zeta_d]$). This cost function is used in the subsequent sections to evaluate the performance of the fluid inerter.

3.4. Determination of optimal tuning ratio and damping coefficient using non-linear optimization

From a preliminary investigation, it is postulated that for a given set of physical parameters/dimensions of the fluid inerter an optimal pair of tuning ratio and damping ratio can be estimated using non-linear optimization methods like SQP. In other words, if the physical dimensions (D_c, D_h, R, l) are fixed, the six-dimensional optimization problem reduces to a two dimensional optimization problem with ($\mathbf{x} = \{\omega_r,\ \zeta_d\}$), with a convex cost function. Thus the problem reduces to a convex optimization problem and tools like SQP can be used. In the following, first, the optimization problem is defined then, the above postulation is verified.

The objective of the optimization problem is to minimize the cost function $\Pi(\mathbf{x})$. The cost function is minimized iteratively by finding the optimal set of parameters in $\mathbf{x}$ that minimizes the cost function in the presence of constraints $H(\mathbf{x})$. Mathematically, the optimal control problem can be written as

$$\begin{aligned} &\min_{\mathbf{x}} \Pi(\mathbf{x}) \\ \text{with:}\quad &\Pi(\mathbf{x}) = \|\mathbf{a}_{rms}^{(1)}\|_\infty \quad \text{from Eq. (22)} \\ \text{s.t.}\quad &H(\mathbf{x}) \geq 0 \end{aligned} \tag{23}$$

where, the constraints are defined as

$$H := \begin{matrix} \omega_r^{\min} \leq \omega_r \leq \omega_r^{\max} \\ \zeta_d^{\min} \leq \zeta_d \leq \zeta_d^{\max} \end{matrix} \tag{24}$$

The optimization problem (OP) is divided into two sub-problems and they are solved separately using specialized methods. The NLP (Non-linear Programming) solver estimates the value of the optimization variables $\mathbf{x}$ at every iteration and sends it to the harmonic balance method (HBM) solver to estimate the cost at the given set of parameters. The estimated cost is then sent to the NLP solver which decides the next point of evaluation. The hierarchy and the communication between the two sub-problems are shown in Fig. 5. Such methods are termed Recursive Elimination methods in the literature. MATLAB's constrained non-linear programming solver `fmincon` has been used to solve the optimal control problem. The optimization problem was solved using a sequential quadratic programming (SQP) algorithm in `fmincon` following [57].

3.4.1. Verifying convexity of the cost function

The postulation on the convexity of the cost function is verified in this section. Four cases are investigated from a low inerter ratio to a high inerter ratio. The cylinder diameter is varied from 1.6 m to 2.0 m and the helix diameter is varied from 0.2 m to 0.35 m while keeping the cylinder length and helix bent radius constant at 1.5 m. This results in four cases as shown in Fig. 6.

The results show that the cost function is indeed a convex function. The global minimum lies along the axis ($\zeta_d \to 0$) at different values of turning ration ω_r depending on the dimensions of the dampers. Thus, the previously made postulation has been verified.

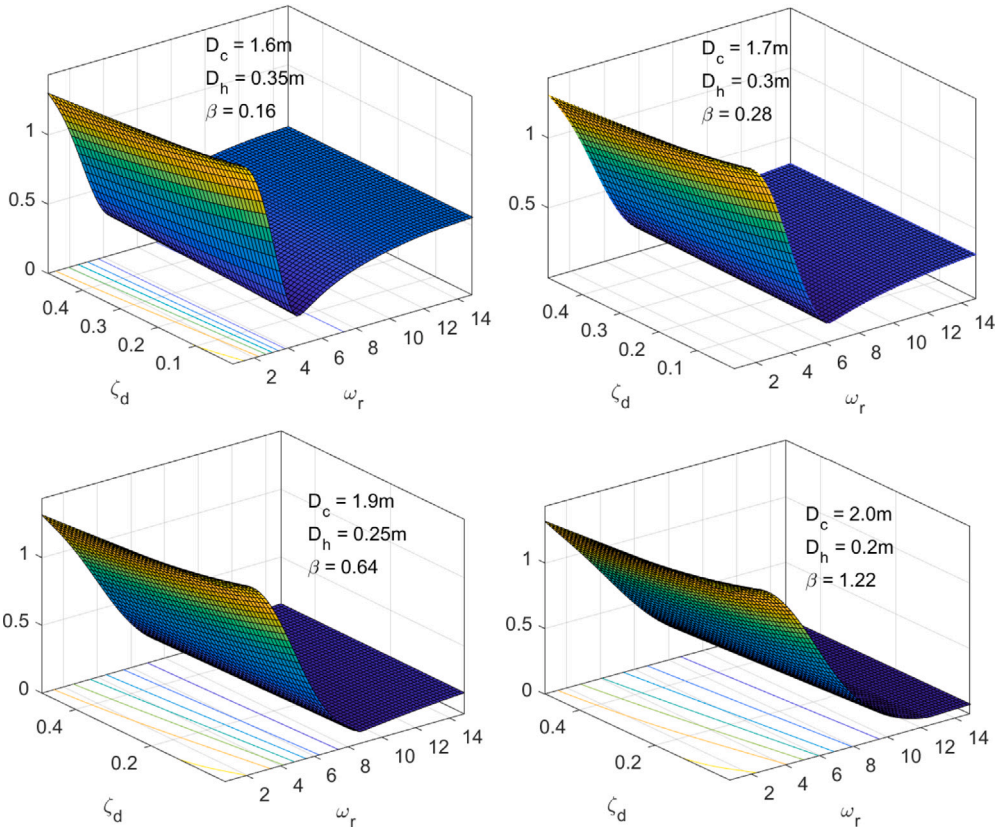

Fig. 6. Solution surface where the z-axis is the cost Π (m).

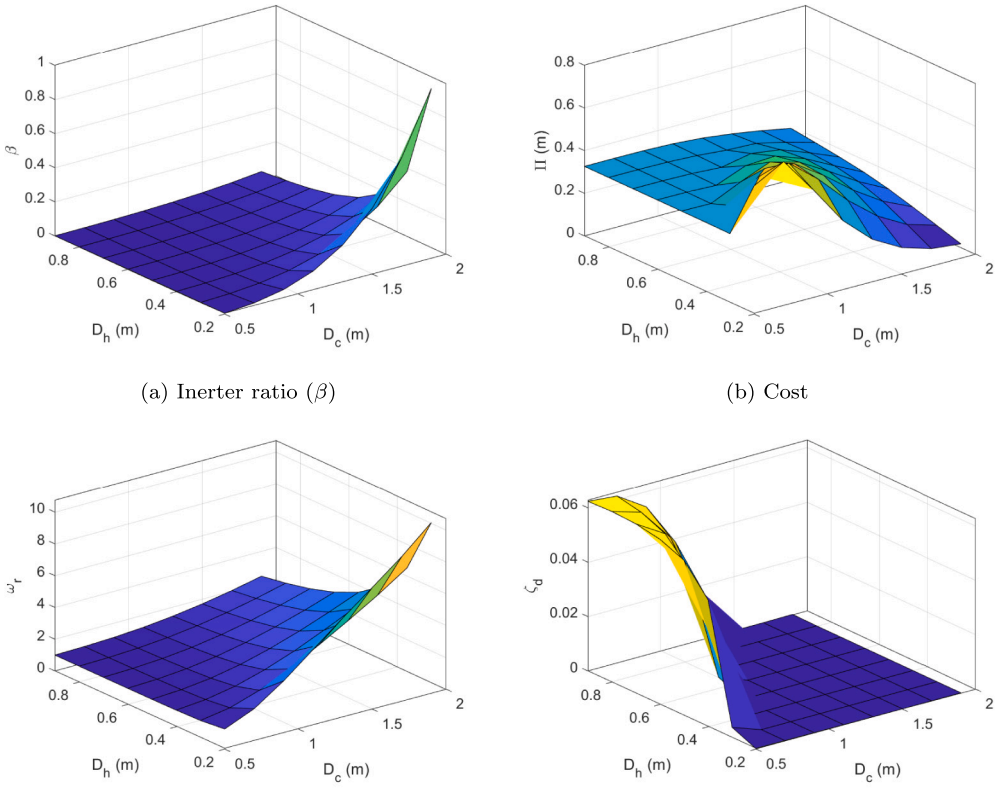

(a) Inerter ratio (β) (b) Cost

(c) Frequency ratio (ω_r) (d) Damping ratio of TMDFI (ζ_d)

Fig. 7. Optimal damper parameters for varying cylinder and helix diameters.

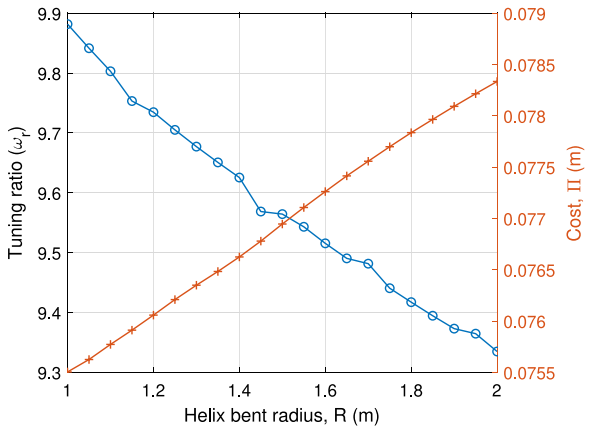

Fig. 8. Damper properties for varying bent radius R.

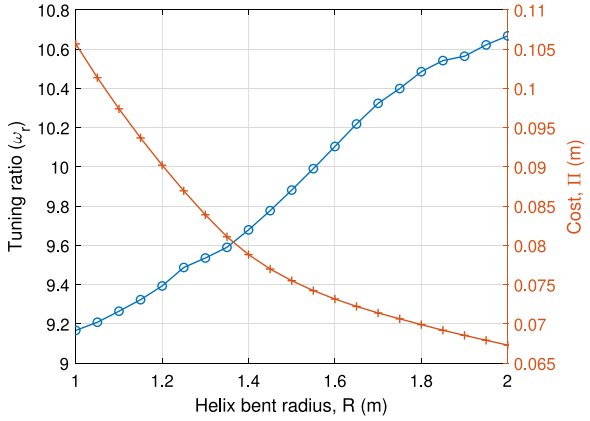

Fig. 9. Damper properties for varying cylinder length l.

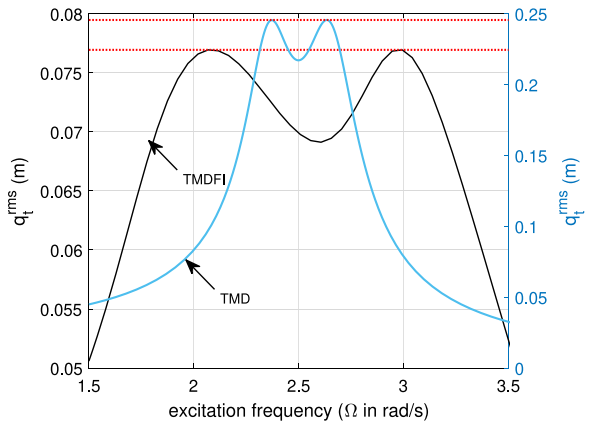

Fig. 10. Comparison against a conventional TMD.

3.5. Parameter optimization of TMDFI

In the previous subsection, a method of finding the optimal tuning ratio and damping coefficient for a dimension-fixed TMDFI was presented. However, the TMDFI has four independent physical parameters that must also be optimized for overall optimum performance. The choice of these physical parameters is largely governed by the desired inertance and damping and is restricted by the practical spatial and weight constraints faced by the design situation. Therefore, the task is to find optimal physical parameters for the fluid inerter for a given spatial and/or weight constraint. The effect of varying the dimensions of the damper is investigated as follows:

1. First, the diameters of the cylinder D_c and the helix D_h are varied and its effect on the optimal frequency ratio, cost function, damping ratio and the resulting inertance ratio is examined using surface plots. The helix bent radius R and the cylinder length l are kept constant at 1 m and 1.5 m respectively. The results are presented in Fig. 7.
2. Next, the bent radius of the helical channel (R) is varied keeping all other parameters constants and its effect on the optimal damping tuning ratio and the cost function is examined. The results are presented in Fig. 8.
3. And lastly, the cylinder length (l) is varied keeping all other parameters constants and its effect on the optimal damping tuning ratio and the cost function is examined. The results are presented in Fig. 9.

The conclusions derived from the results are as follows:

1. The diameters of the cylinder and the helical channel have the most significant effect on the inertance and the parasitic damping of the fluid inerter (refer to Eqs. (13) and (14) respectively). A larger diameter of the cylinder and a smaller diameter of the helix leads to a greater inerter ratio.
2. Naturally, a higher inerter ratio results in a smaller cost (smaller peak of the frequency response curve).
3. The optimal tuning ratio increases with increasing inerter ratio which is supported by previous experience (see [36]).
4. The required primary damping of the TMDFI is negligible as shown in Fig. 7(d) and the parasitic damping is sufficient at a high inerter ratio.
5. Fig. 8 shows that increasing the bent radius of the helix can deteriorate performance of the damper. However, due to physical restrictions $R \geq \frac{D_c+D_h}{2}$.
6. Increasing the length of the cylinder (l) has similar effect on the TMDFI as the area ratio (A_c/A_h); refer Eq. (13) and (14) as shown in Fig. 9. However, again it is important to note here that increasing the length of the cylinder considerably increases the weight and dimensions of the device and must be considered with caution.

As mentioned earlier, the choice of the physical parameters is restricted by the spatial and/or weight restrictions in place. Sarkar and Fitzgerald [36] showed that for floating offshore wind turbines it is not ideal to simply increase the mass of the damper to attain better performance. The increased mass on top of the tower can destabilize the platform and cause excessive vibrations. Therefore, in this paper, the final parameter is chosen so that the additional weight of the fluid is less than 1% of the weight of the tower. Therefore, the total of the TMD mass and fluid inerter is $\approx 2\%$ of the mass of the tower. The frequency response of the tower coupled with the TMDFI is compared with a optimized classical TMD with a 2% mass ratio and is presented in Fig. 10. It can be clearly observed that with similar mass ratios, the TMDFI performs considerably better than a classical TMD. This clearly emphasizes the advantages of the inerter action.

In the following section the results of a fully non-linear floating offshore wind turbine coupled with the designed TMDFI is presented.

4. Vibration mitigation of a 5MW floating wind turbine

The 5 MW spar-type offshore reference wind turbine defined by NREL in [58] is used here to numerically evaluate the performance of the TMDFI installed on a full-scale 5 MW FOWT as shown in Fig. 2. The codes for the offshore wind turbine are developed in MATLAB [59]. The aerodynamic loads are estimated using Blade Element Momentum theory [60]; the hydrodynamic forces are estimated using Morison's

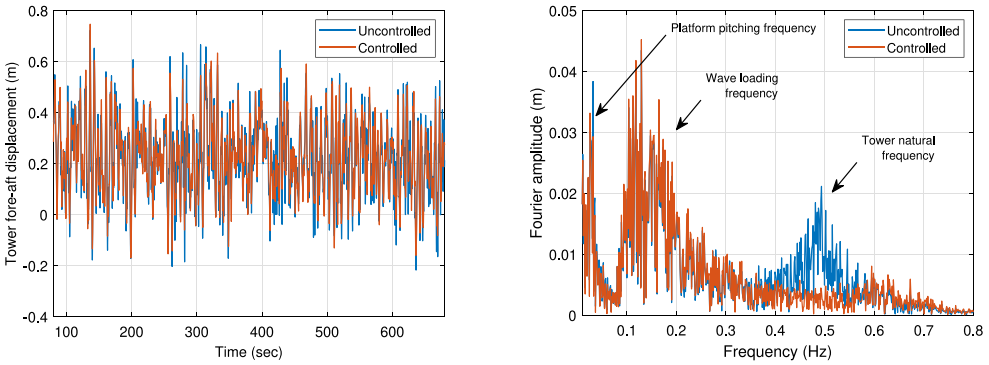

(a) Time history (b) Fourier spectrum

Fig. 11. Load Case 1.1: Tower fore–aft displacement.

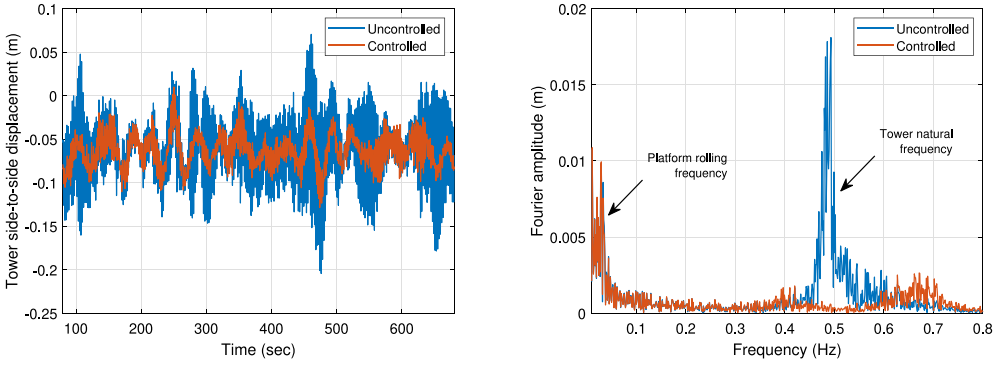

(a) Time history (b) Fourier spectrum

Fig. 12. Load Case 1.1: Tower side-to-side displacement.

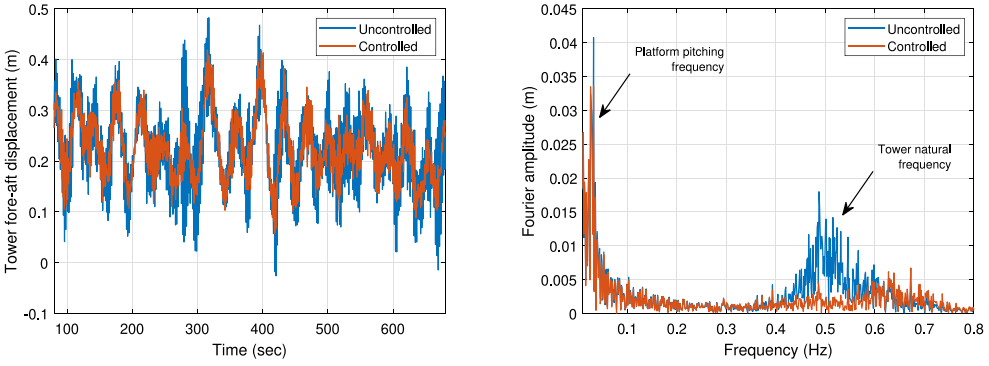

(a) Time history (b) Fourier spectrum

Fig. 13. Load Case 1.2: Tower fore–aft displacement.

equations [36], and mooring cables are modelled using the open-source software MoorDyn [61]. All cases are simulated for a standard 600 s (excluding initial transience) and with a sampling rate of 40 Hz. The numerical Runge–Kutta method 'ODE 4' is used for time integration of the non-linear system. The turbulent wind fields are generated using the TurbSim [62] package distributed by NREL. It has the capability of generating turbulent 3-D wind field taking into account wind shear and spatial coherence. IEC [63] Normal turbulence model (NTM) with turbine class A is used to model the atmospheric turbulence. The stochastic sea is modelled using the Pierson–Moskowitz spectrum [64]. For more details please refer [23,44] (see Figs. 12–19).

The chosen damper parameters are summarized in Table 1. It must be noted here, that the optimal design renders linear damping ratio $\zeta_d \to 0$. This changes the initial damper configuration by removing the linear damper. All numerical simulations in this section are performed with $\zeta_d = 0$ i.e., without the linear dashpot. The choice of the fluid inerter dimensions results in a inerter ratio β of 0.715. It has been shown in [36] that the performance of a inerter-based damper saturates above a inerter ratio of 0.6–0.8. Hence, a β of 0.715 suffices as there will be no significant benefit from any further increase.

In this paper, the performance of the damper under three met-ocean scenarios are investigated. The cases are listed as follows

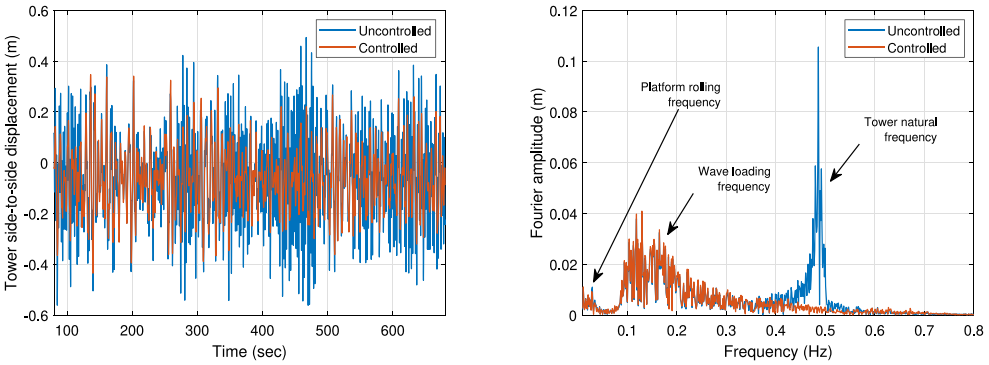

(a) Time history (b) Fourier spectrum

Fig. 14. Load Case 1.2: Tower side-to-side displacement.

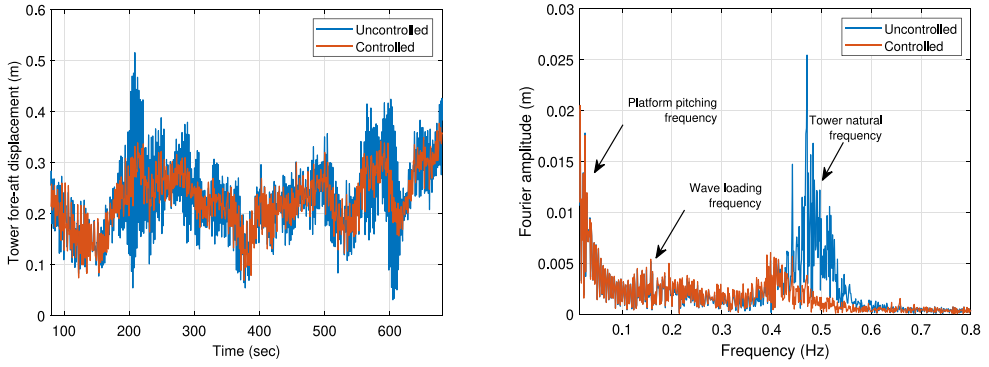

(a) Time history (b) Fourier spectrum

Fig. 15. Load Case 2.1: Tower fore–aft displacement.

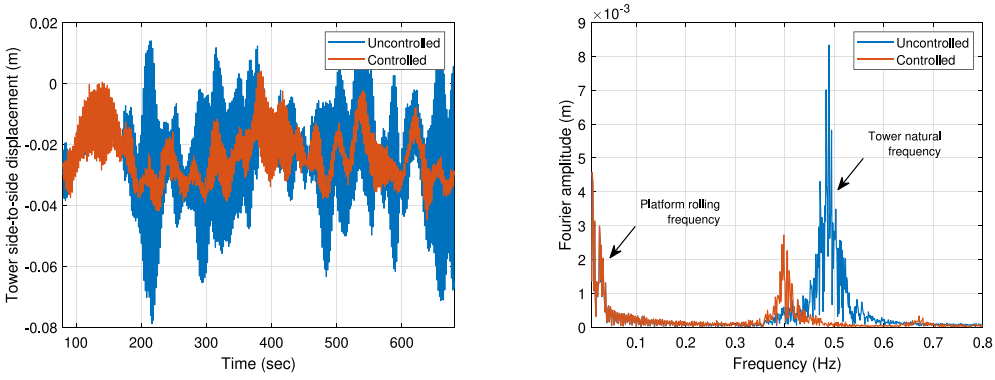

(a) Time history (b) Fourier spectrum

Fig. 16. Load Case 2.1: Tower side-to-side displacement.

1 Violent met-ocean conditions — high wind speeds are accompanied by large wave heights. In this case, the significant wave height is assumed to be 6 m, the peak spectral period as 8 s and the hub-height mean wind speed as 20 m/s.
2 Calm met-ocean conditions — low wind speeds are accompanied by small wave heights. In this case, the significant wave height is assumed to be 0.75 m, the peak spectral period as 6 s and the hub-height mean wind speed as 8 m/s.
3 Near resonance — wind speed at which the 3P frequency of the aerodynamic loads is close to the natural frequency of the tower. In this case, the tower's natural frequency matches the 3p frequency when 3p ≈ 0.4885 Hz ⇒ p ≈ 0.163 Hz; i.e., at a rotor speed of ≈ 9.78 rpm that roughly occurs at a wind speed of 8.8 m/s.

The performance of the controller in reducing the tower-top fore–aft and side-to-side vibrations for all the assumed load cases are shown in Fig. 11 through Fig. 20. The time histories of the tower-top displacements along with their Fourier spectrum are represented in these figures. It can be clearly observed that the damper is capable of dissipating the energy associated with the tower's natural frequency very effectively. It can also be observed that the tower-top vibrations have more than one frequency content. When the wave direction is aligned with the tower vibration mode under consideration, there

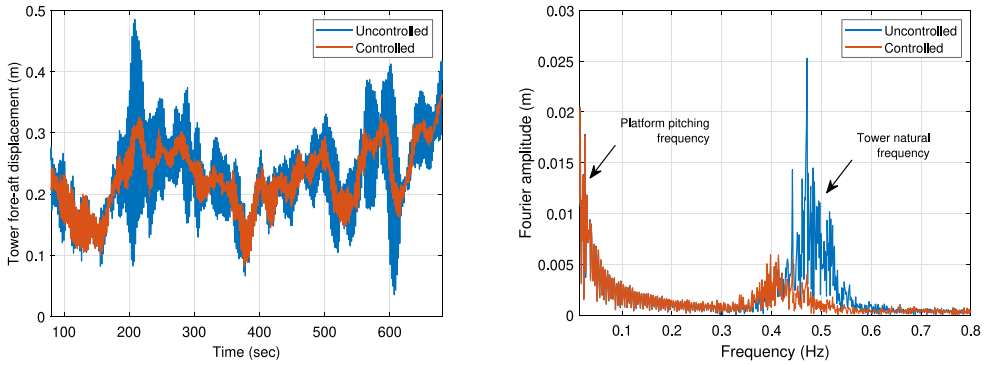

(a) Time history (b) Fourier spectrum

Fig. 17. Load Case 2.2: Tower fore–aft displacement.

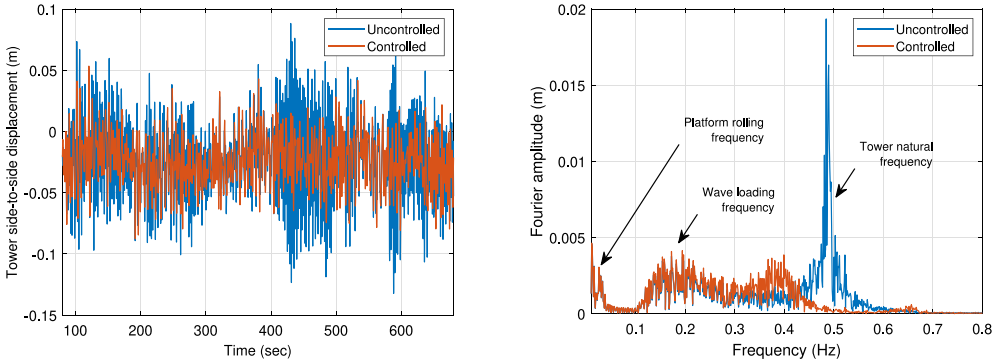

(a) Time history (b) Fourier spectrum

Fig. 18. Load Case 2.2: Tower side-to-side displacement.

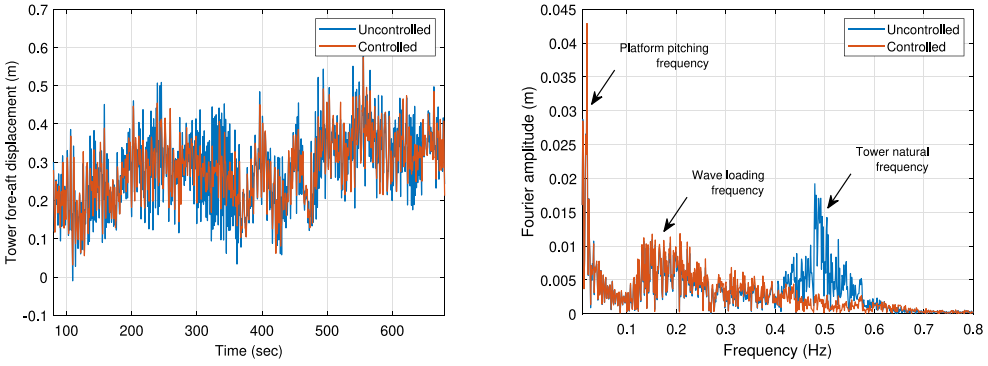

(a) Time history (b) Fourier spectrum

Fig. 19. Load Case 3: Tower fore–aft displacement.

is a significant amount of energy associated with the wave loading frequency. The tower-top vibrations are also affected by the platform pitching and rolling frequency in the fore–aft and side-to-side directions respectively. Quantitatively, the performance of the controller in terms of reduction in root mean square tower-top displacements are presented in Tables 2 and 3. The TMDFI demonstrates impressive vibration mitigation capabilities by achieving a significant reduction in tower-top vibrations. The load cases used in this paper are intentionally chosen to be consistent with the ones used in [36] so that a comparison can be made between the "ideal" TMDI and the TMDFI presented in this paper. Comparing the two, the TMDFI performs as good as the "ideal" TMDI. This is particularly encouraging since the design and maintenance of a fluid inerter is simpler than cheaper than an "ideal" mechanical inerter.

The reduction of TMD stroke is also investigated in this paper. The stroke of the tuned damper mass with and without the fluid-inerter (classical TMD) for load cases 1.1 and 1.2 are shown in Figs. 21(a) and 21(b) respectively. As expected, it is observed that the TMD

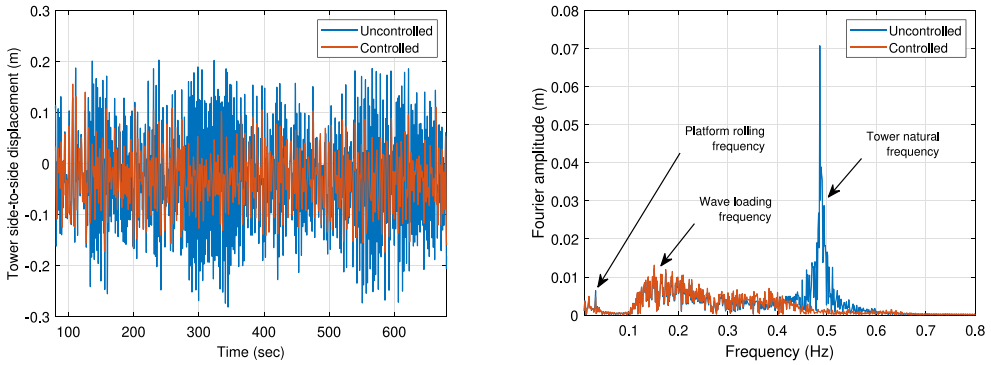

(a) Time history (b) Fourier spectrum

Fig. 20. Load Case 3: Tower side-to-side displacement.

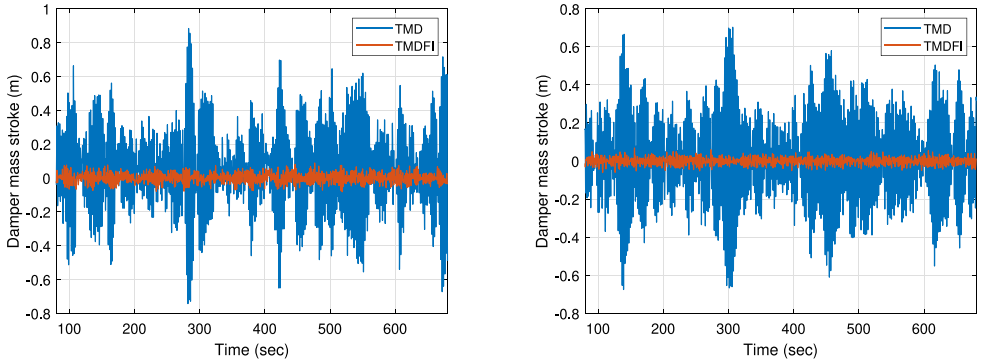

(a) Load Case 1.1: Damper coupled in fore-aft direction (b) Load Case 1.2: Damper coupled in side-to-side direction

Fig. 21. Comparison of damper stroke.

Table 2
Reduction in tower-top side-to-side displacements.

LC #	Description	U_w (m/s)	H_s (m)	T_p (sec)	Wave dir. (deg.)	P.R (%)	S.R (%)
1.1	Violent met-ocean condition; high wind speeds with large wave heights	20	6	8	0	53	91
1.2					90	28	90
2.1	Calm met-ocean condition; low wind speeds with small wave heights	8	0.75	6	0	44	95
2.2					90	33	94
3	Resonance of tower with aerodynamic loads	8.8	2.25	6.25	90	42	94

U_w = Hub-height mean wind speed
H_s = Significant wave height
T_p = Wave period
$S.R$ = Percentage reduction in maximum amplitude of TMD stroke
$P.R$ = Percentage reduction in tower-top rms displacement.

stroke is significantly reduced. The percentage reductions in maximum TMD stroke are enlisted in Tables 2 and 3 and is comparable to the "ideal" inerter presented in [36]. This feature is very attractive for a damper designed for wind turbines as there are strict spatial constraints imposed on them.

5. Conclusion

In this paper, the use of a fluid inerter for vibration control of floating offshore wind turbine towers was demonstrated. The results presented in the paper clearly show that there is great potential for such devices in multi-megawatt FOWTs. As this type of device is used for the first time for vibration control of FOWT towers, the majority of the paper was devoted to the design of the controller to provide insight and guidance into the behaviour of the fluid-inerter. An extended harmonic balance method was used to study the frequency response of the non-linear tower–damper coupled system and then non-linear optimization methods were used to optimize the frequency response of the coupled system to achieve maximum vibration reduction. Conclusions are drawn here on the two aspects dealt with in this paper; (i) on the design of the TMDFI and (ii) on its performance on a 5MW floating wind turbine.

The important conclusions on the design of the controller are

1. The tower-TMDFI optimization problem is a six-dimensional optimization problem. Gradient-based optimization tools are not

Table 3
Reduction in tower-top fore–aft displacements.

LC #	Description	U_w (m/s)	H_s (m)	T_p (sec)	Wave dir. (deg.)	P.R (%)	S.R (%)
1.1	Violent met-ocean condition; high wind speeds with large wave heights	20	6	8	0	5	86
1.2					90	23	91
2.1	Calm met-ocean condition; low wind speeds with small wave heights	8	0.75	6	0	22	95
2.2					90	23	96
3	Resonance of tower with aerodynamic loads	8.8	2.25	6.25	90	11	90

U_w = Hub-height mean wind speed
H_s = Significant wave height
T_p = Wave period
$S.R$ = Percentage reduction in maximum amplitude of TMD stroke
$P.R$ = Percentage reduction in tower-top rms displacement
$\phi = 0.5$.

capable of optimizing the fluid-inerter due to the presence of multiple local minima in the solution hyperplane.
2. However, with a fixed physical dimension of the fluid-inerter the optimization, reduces from a six-dimensional problem to a two-dimensional problem and gradient-based convex optimization tools can be used to find the global minima.
3. The inerter ratio and the required tuning ratio increases with increasing cylinder diameter (D_c) to the helical channel diameter (D_h) ratio.
4. At high inerter ratios there is no need for an additional linear damper and the quadratic damping offered by the fluid inerter is sufficient for optimum performance.
5. The performance of the controller improves with increasing inertance ratio, length of the cylinder and helix bent radius.
6. However, the dimensions of the fluid inerter is normally limited by the spatial/weight restrictions inside a wind turbine. In this paper, the weight of the fluid inerter has been limited to 1% of the tower mass.

Important conclusions drawn from the application of the TMDFI installed in the tower of a 5MW FOWT are as follows

1. The TMDFI offers great potential in vibration mitigation for floating offshore wind turbine towers. This novel damper performs significantly better than the traditional TMD and comparable to an "ideal" mechanical inerter.
2. The inerter also greatly reduces the displacement of the tuned mass (reduction in TMD stroke) as a by-product. This a significant advantage over traditional TMDs in places with strict spatial restrictions. Since the space available inside a wind turbine tower is very limited, the reduction in the damper stroke is an extremely beneficial and practical advantage over classical TMDs for application in FOWTs.

CRediT authorship contribution statement

Saptarshi Sarkar: Conceptualization, Data curation, Formal analysis, Investigation, Methodology, Software, Writing – original draft, Writing – review & editing. **Breiffni Fitzgerald:** Conceptualization, Data curation, Formal analysis, Investigation, Methodology, Software, Writing – original draft, Writing – review & editing.

Declaration of competing interest

The authors declare that they have no known competing financial interests or personal relationships that could have appeared to influence the work reported in this paper.

Appendix

Degrees of freedom:

q_{Sg}	Platform surge
q_{Sw}	Platform sway
q_{Hv}	Platform heave
q_R	Platform roll
q_P	Platform pitch
q_Y	Platform yaw
q_{TFA1}	First tower fore–aft bending mode
q_{TFA2}	Second tower fore–aft bending mode
q_{TSS1}	First tower side-to-side bending mode
q_{TSS2}	Second tower side-to-side bending mode
q_{yaw}	Nacelle yaw

q_{GeAz}	Generator azimuth angle
q_{DrTr}	Drive-train torsional flexibility
q_{BiF1}	First flapwise bending mode for ith blade
q_{BiF2}	Second flapwise bending mode for ith blade
q_{BiE1}	First edgewise bending mode for ith blade
q_D	Damper

References

[1] Global wind report. 2019, Global Wind Energy Council.
[2] Future of wind: deployment, investment, technology, grid integration and socio-economic aspects. International Renewable Energy Agency; 2019.
[3] Oh K-Y, Nam W, Ryu MS, Kim J-Y, Epureanu BI. A review of foundations of offshore wind energy convertors: Current status and future perspectives. Renew Sustain Energy Rev 2018;88:16–36.
[4] Dueñas-Osorio L, Basu B. Unavailability of wind turbines due to wind-induced accelerations. Eng Struct 2008;30(4):885–93.
[5] Fitzgerald B, Sarkar S, Staino A. Improved reliability of wind turbine towers with active tuned mass dampers (ATMDs). J Sound Vib 2018;419:103–22.
[6] Dinh V-N, Basu B. Passive control of floating offshore wind turbine nacelle and spar vibrations by multiple tuned mass dampers. Struct Control Health Monit 2015;22(1):152–76.
[7] Yang J, He E. Coupled modeling and structural vibration control for floating offshore wind turbine. Renew Energy 2020.
[8] Si Y, Karimi HR, Gao H. Modelling and optimization of a passive structural control design for a spar-type floating wind turbine. Eng Struct 2014;69:168–82.
[9] Stewart GM, Lackner MA. The impact of passive tuned mass dampers and wind–wave misalignment on offshore wind turbine loads. Eng Struct 2014;73:54–61.
[10] Zhang Z, Høeg C. Vibration control of floating offshore wind turbines using liquid column dampers. In: The science of making torque from wind (TORQUE 2018) European academy of wind energy: the science of making Torque from wind. Vol. 1037. 2018.
[11] Jahangiri V, Sun C. Three-dimensional vibration control of offshore floating wind turbines using multiple tuned mass dampers. Ocean Eng 2020;206:107196.
[12] Sun C, Jahangiri V. Bi-directional vibration control of offshore wind turbines using a 3D pendulum tuned mass damper. Mech Syst Signal Process 2018;105:338–60.

[13] Dinh V-N, Basu B, Nagarajaiah S. Semi-active control of vibrations of spar type floating offshore wind turbines. Smart Struct Syst 2016;18(4):683–705.
[14] Karimi HR, Zapateiro M, Luo N. Semiactive vibration control of offshore wind turbine towers with tuned liquid column dampers using H output feedback control. In: 2010 IEEE international conference on control applications. IEEE; 2010, p. 2245–9.
[15] Sarkar S, Chakraborty A. Optimal design of semiactive MR-TLCD for along-wind vibration control of horizontal axis wind turbine tower. Struct Control Health Monit 2018;25(2):e2083.
[16] Sun C. Semi-active control of monopile offshore wind turbines under multi-hazards. Mech Syst Signal Process 2018;99:285–305.
[17] Lackner MA, Rotea MA. Structural control of floating wind turbines. Mechatronics 2011;21(4):704–19. http://dx.doi.org/10.1016/j.mechatronics.2010.11.007, URL: http://www.sciencedirect.com/science/article/pii/S0957415810002072.
[18] Fitzgerald B, Basu B, Nielsen SRK. Active tuned mass dampers for control of in-plane vibrations of wind turbine blades. Struct Control Health Monit 2013;20(12):1377–96. http://dx.doi.org/10.1002/stc.1524.
[19] Fitzgerald B, Basu B. Cable connected active tuned mass dampers for control of in-plane vibrations of wind turbine blades. J Sound Vib 2014;333(23):5980–6004.
[20] Fitzgerald B, Basu B. Structural control of wind turbines with soil structure interaction included. Eng Struct 2016;111:131–51.
[21] Hu Y, He E. Active structural control of a floating wind turbine with a stroke-limited hybrid mass damper. J Sound Vib 2017;410:447–72.
[22] Fitzgerald B, Staino A, Basu B. Wavelet-based individual blade pitch control for vibration control of wind turbine blades. Struct Control Health Monit 2019;26(1):e2284.
[23] Sarkar S, Chen L, Fitzgerald B, Basu B. Multi-resolution wavelet pitch controller for spar-type floating offshore wind turbines including wave-current interactions. J Sound Vib 2020;115170.
[24] Sarkar S, Fitzgerald B, Basu B. Individual blade pitch control of floating offshore wind turbines for load mitigation and power regulation. IEEE Trans Control Syst Technol 2020.
[25] Zhang Z, Nielsen S, Blaabjerg F, Zhou D. Dynamics and control of lateral tower vibrations in offshore wind turbines by means of active generator torque. Energies 2014;7(11):7746–72.
[26] Smith MC. Synthesis of mechanical networks: the inerter. In: Decision and control, 2002, proceedings of the 41st IEEE conference on. Vol. 2. IEEE; 2002, p. 1657–62.
[27] Ikago K, Saito K, Inoue N. Seismic control of single-degree-of-freedom structure using tuned viscous mass damper. Earthq Eng Struct Dyn 2012;41(3):453–74.
[28] Garrido H, Curadelli O, Ambrosini D. Improvement of tuned mass damper by using rotational inertia through tuned viscous mass damper. Eng Struct 2013;56:2149–53.
[29] Lazar I, Neild S, Wagg D. Using an inerter-based device for structural vibration suppression. Earthq Eng Struct Dyn 2014;43(8):1129–47.
[30] Hu Y, Chen MZ. Performance evaluation for inerter-based dynamic vibration absorbers. Int J Mech Sci 2015;99:297–307.
[31] Zhang R, Zhao Z, Dai K. Seismic response mitigation of a wind turbine tower using a tuned parallel inerter mass system. Eng Struct 2019;180:29–39.
[32] Zhang Z, Larsen TG. Optimal calibration of the rotational inertia double tuned mass damper (RIDTMD) for rotating wind turbine blades. J Sound Vib 2020;115827.
[33] Zhang Z, Fitzgerald B. Tuned mass-damper-inerter (TMDI) for suppressing edgewise vibrations of wind turbine blades. Eng Struct 2020;221:110928.
[34] Ma R, Bi K, Hao H. A novel rotational inertia damper for heave motion suppression of semisubmersible platform in the shallow sea. Struct Control Health Monit 2019;e2368.
[35] Hu Y, Wang J, Chen MZ, Li Z, Sun Y. Load mitigation for a barge-type floating offshore wind turbine via inerter-based passive structural control. Eng Struct 2018;177:198–209.
[36] Sarkar S, Fitzgerald B. Vibration control of spar-type floating offshore wind turbine towers using a tuned mass-damper-inerter. Struct Control Health Monit 2020;27(1):e2471.
[37] Swift S, Smith MC, Glover A, Papageorgiou C, Gartner B, Houghton NE. Design and modelling of a fluid inerter. Internat J Control 2013;86(11):2035–51.
[38] De Domenico D, Deastra P, Ricciardi G, Sims ND, Wagg DJ. Novel fluid inerter based tuned mass dampers for optimised structural control of base-isolated buildings. J Franklin Inst B 2019;356(14):7626–49.
[39] De Domenico D, Ricciardi G, Zhang R. Optimal design and seismic performance of tuned fluid inerter applied to structures with friction pendulum isolators. Soil Dyn Earthq Eng 2020;132:106099.
[40] Gonzalez-Buelga A, Lazar IF, Jiang JZ, Neild SA, Inman DJ. Assessing the effect of nonlinearities on the performance of a tuned inerter damper. Struct Control Health Monit 2017;24(3):e1879.
[41] Liu X, Jiang JZ, Titurus B, Harrison A. Model identification methodology for fluid-based inerters. Mech Syst Signal Process 2018;106:479–94.
[42] Kane TR, Levinson DA. Dynamics, theory and applications. McGraw Hill; 1985.
[43] Jonkman J, Buhl Jr M. FAST user's guide. Technical report No. NREL/EL-500-38230, Golden, CO: National Renewable Energy Laboratory; 2005.
[44] Sarkar S. Individual blade pitch control strategies for spar-type floating offshore wind turbines (Ph.D. thesis), Trinity College Dublin; 2020.
[45] Sarkar S, Fitzgerald B. Use of kane's method for multi-body dynamic modelling and control of spar-type floating offshore wind turbines. Energies 2021;14(20):6635.
[46] Stewart G, Lackner M. Offshore wind turbine load reduction employing optimal passive tuned mass damping systems. IEEE Trans Control Syst Technol 2013;21(4):1090–104.
[47] Basu B, Zhang Z, Nielsen SR. Damping of edgewise vibration in wind turbine blades by means of circular liquid dampers. Wind Energy 2016;19(2):213–26.
[48] Colwell S, Basu B. Tuned liquid column dampers in offshore wind turbines for structural control. Eng Struct 2009;31(2):358–68. http://dx.doi.org/10.1016/j.engstruct.2008.09.001, URL: http://www.sciencedirect.com/science/article/pii/S0141029608003076.
[49] Lackner MA, Rotea MA. Passive structural control of offshore wind turbines. Wind Energy 2011;14(3):373–88.
[50] Zhang Z-L, Chen J-B, Li J. Theoretical study and experimental verification of vibration control of offshore wind turbines by a ball vibration absorber. Struct Infrastruct Eng 2014;10(8):1087–100.
[51] Marian L, Giaralis A. Optimal design of a novel tuned mass-damper-inerter (TMDI) passive vibration control configuration for stochastically support-excited structural systems. Probab Eng Mech 2014;38:156–64.
[52] Giaralis A, Petrini F. Wind-induced vibration mitigation in tall buildings using the tuned mass-damper-inerter. J Struct Eng 2017;143(9):04017127.
[53] Yang J, He E, Hu Y. Dynamic modeling and vibration suppression for an offshore wind turbine with a tuned mass damper in floating platform. Appl Ocean Res 2019;83:21–9.
[54] He E-M, Hu Y-Q, Zhang Y. Optimization design of tuned mass damper for vibration suppression of a barge-type offshore floating wind turbine. Proc Inst Mech Eng M J Eng Marit Environ 2017;231(1):302–15.
[55] Krack M, Gross J. Harmonic balance for nonlinear vibration problems. Springer; 2019.
[56] Seydel R. Practical bifurcation and stability analysis. Vol. 5. Springer Science & Business Media; 2009.
[57] Nocedal J, Wright S. Numerical optimization. Springer Science & Business Media; 2006.
[58] Jonkman JM. Definition of the floating system for phase IV of OC3. 2010.
[59] MATLAB. version 9.4.0 (R2018a). Natick, Massachusetts: The MathWorks Inc. 2018.
[60] Ning SA. A simple solution method for the blade element momentum equations with guaranteed convergence. Wind Energy 2014;17(9):1327–45.
[61] Hall M. MoorDyn user's guide. Orono, ME: Department of Mechanical Engineering, University of Maine; 2015.
[62] Jonkman BJ. TurbSim user's guide: version 1.50. Tech. rep., Golden, CO (United States): National Renewable Energy Lab.(NREL); 2009.
[63] IEC 61400-1: wind turbines part 1: design requirements. International Electrotechnical Commission; 2005.
[64] Pierson Jr WJ, Moskowitz L. A proposed spectral form for fully developed wind seas based on the similarity theory of SA kitaigorodskii. J Geophys Res 1964;69(24):5181–90.